Distinguishing spins in decay chains with photons at the Large Hadron Collider

Ehrenfeld, W ; Freitas, A ; Landwehr, A ; Wyler, D

Abstract: Several models for physics beyond the Standard Model predict new particles with a decay signature including hard photons and missing energy. Two well-motivated examples are supersymmetry with gauge-mediated breaking (GMSB) and the standard model with two universal extra dimensions. Both models lead to decay chains with similar collider signatures, including hard photon emission. The main discriminating feature are the spins of the new particles. In this paper we discuss how information about the spins of the particles can be extracted from lepton-photon or quark-photon invariant mass distributions at the Large Hadron Collider. The characteristic shapes of the distributions are derived analytically and then studied in a realistic Monte-Carlo simulation. We find that for a typical GMSB mass spectrum with particle masses below 1 TeV, already 10 fb−1 integrated luminosity at 14 TeV center-of-mass energy are sufficient to discriminate the two models with high significance.

DOI: https://doi.org/10.1088/1126-6708/2009/07/056

Preprint typeset in JHEP style - HYPER VERSION

Distinguishing spins in decay chains with photons at the Large Hadron Collider

Wolfgang Ehrenfeld

DESY, Hamburg, Notkestr. 85, D-22603 Hamburg, Germany
E-mail: wolfgang.ehrenfeld@desy.de

Ayres Freitas

Department of Physics & Astronomy, University of Pittsburgh, 3941 O'Hara St, Pittsburgh, PA 15260, USA
E-mail: afreitas@pitt.edu

Ananda Landwehr*, Daniel Wyler

Institut für Theoretische Physik, Universität Zürich, Winterthurerstrasse 190, CH-8057 Zürich, Switzerland
E-mail: landwehr@mppmu.mpg.de, wyler@physik.uzh.ch

Abstract: Several models for physics beyond the Standard Model predict new particles with a decay signature including hard photons and missing energy. Two well-motivated examples are supersymmetry with gauge-mediated breaking (GMSB) and the standard model with two universal extra dimensions. Both models lead to decay chains with similar collider signatures, including hard photon emission. The main discriminating feature are the spins of the new particles. In this paper we discuss how information about the spins of the particles can be extracted from lepton-photon or quark-photon invariant mass distributions at the Large Hadron Collider. The characteristic shapes of the distributions are derived analytically and then studied in a realistic Monte-Carlo simulation. We find that for a typical GMSB mass spectrum with particle masses below 1 TeV, already 10 fb^{-1} integrated luminosity at 14 TeV center-of-mass energy are sufficient to discriminate the two models with high significance.

Keywords: Supersymmetry Phenomenology.

*Current address: Max-Planck-Institut für Physik, Föhringer Ring 6, D-80805 München, Germany

Contents

1. Introduction **1**

2. Spin correlations in GMSB and UED6 **2**
- 2.1 Spin correlations in GMSB 5
- 2.2 Spin correlations in UED6 6
- 2.3 Discussion of analytical results 7

3. Monte-Carlo simulation and numerical analysis **8**
- 3.1 Cross Sections 11
- 3.2 χ^2 Analysis 12

4. Conclusion **13**

A. Analytical results for invariant mass distributions **16**

1. Introduction

Several models for physics beyond the Standard Model (SM) introduce partner particles for all SM particles, the lightest of which is stable and could be the constituent of dark matter. The best known examples are supersymmetry (SUSY) with conserved R-parity and universal extra dimensions (UED) with conserved Kaluza-Klein (KK) parity [1]. Since the observable signatures for these models at the Large Hadron Collider (LHC) look quite similar [2], it will be important to test the fundamental quantum numbers of the new particles in order to scrutinize the nature of the underlying physics.

For example, both SUSY and UED require that the couplings of the new particles are identical to the corresponding couplings of their SM partners; a prediction which can be tested at the LHC by measuring cross section ratios [3]. However, a crucial distinction between the two models is given by the spins of the new particles. While the SUSY partners differ from their SM counterparts by one half-unit of spin, the KK excitations in UED have the same spin as their SM partners. Recently, extensive work has been performed to determine the spins of SUSY or UED particles by exploiting angular correlations in the decay of those particles at the LHC[1]. Many papers have focused on decay chains involving lepton pairs [5, 6, 7, 8, 9, 10, 11]. A typical example of such a decay chain in SUSY is $\tilde{q} \to q\,\tilde{\chi}_2^0 \to q\,l^+l^-\,\tilde{\chi}_1^0$. Other studies have examined channels involving heavy gauge bosons [9, 12, 13, 14], sleptons [15, 13] and top quarks. However, in all of the existing studies it

[1] A few studies have explored more model-dependent discrimination methods based on total cross sections [4] and higher KK modes [6].

was assumed that the lightest new particle is either a neutralino or weak vector boson in SUSY or UED, respectively.

In this article the spin determination from angular correlations is extended to decay chains that involve hard photons in the final state. Such decay channels occur naturally in gauge-mediated supersymmetry breaking (GMSB), where the lightest SUSY particle is the gravitino [17], as well as in the extension of the SM by two universal extra dimensions (UED6), where the lightest KK mode is typically a scalar component of a higher-dimensional vector boson, called "scalar adjoint" [18, 19, 20]. It has been shown earlier that a high-energy e^+e^- collider could distinguish between GMSB and UED6 by studying angular correlations in pair production and decay of the selectron (KK-electrons) and neutralinos (KK-gauge bosons) [21]. The purpose of the present paper is to study how such a distinction can be achieved at the LHC by analyzing decay chains involving leptons and photons. In particular, we are investigating how the spin of the lightest new particle, which escapes from the detector in form of missing momentum, can be inferred from invariant mass distributions of the leptons and photons.

In section 2 we describe analytical calculations of the relevant invariant mass distributions and compare the angular correlations predicted by GMSB and UED6. In order to evaluate the prospects for experimental measurements of these distributions, we present in section 3 results of a realistic Monte-Carlo simulation, incorporating the spin correlation effects of the two models. We present our conclusions in section 4. The detailed analytical results are collected in the appendix.

2. Spin correlations in GMSB and UED6

In our notations and conventions we follow Ref. [22] for supersymmetry and Ref. [18, 19, 20] for the Standard Model in six dimensions (UED6).

GMSB is a promising candidate for a mechanism that generates TeV-scale masses for the SUSY partners, most notably since it explains the absence of large flavor-changing neutral currents. In GMSB, the lightest SUSY particle is typically the gravitino $\tilde{G}$, with a mass $m_{\tilde{G}} \lesssim 1$ MeV. If the next-to-lightest SUSY particle is a neutralino, it will mostly decay into the gravitino and a photon, $\tilde{\chi}_1^0 \to \gamma \tilde{G}$. Depending on the neutralino mass, there could be a smaller branching fraction into a Z boson, which we will not investigate further.

In UED6, the lightest particle at KK level (1,0) is typically the scalar adjoint of the hypercharge boson, $B_H^{(1,0)}$ [19, 23]. The vector mode of the KK-hypercharge boson, $B_\mu^{(1,0)}$, can decay into the scalar adjoint via a loop-induced process, $B_\mu^{(1,0)} \to \gamma\, B_H^{(1,0)}$. This decay mode has a sizable branching fraction of about 34% [20]. Therefore the two models lead to very similar decay signatures. In particular, the decay chain

$$\tilde{\chi}_2^0 \to l^\pm\, \tilde{l}_{\rm R}^\mp \to l^+l^-\, \tilde{\chi}_1^0 \to l^+l^-\, \gamma\, \tilde{G}\,, \tag{2.1}$$

which is typical in GMSB, is imitated by the equivalent process in UED6,

$$Z_\mu^{(1,0)} \to l^\pm\, L_+^{(1,0)} \to l^+l^-\, B_\mu^{(1,0)} \to l^+l^-\, \gamma\, B_H^{(1,0)}\,, \tag{2.2}$$

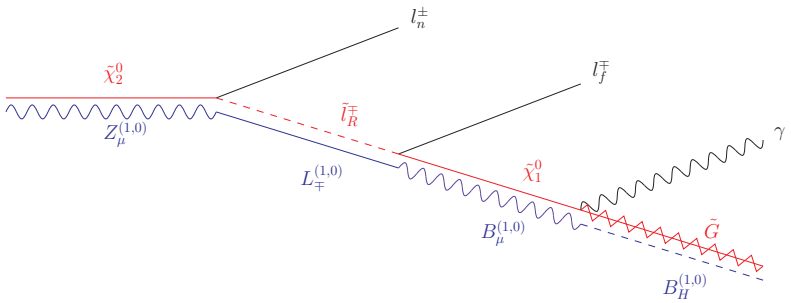

Figure 1: *SUSY (red/top) and UED6 (blue/bottom) decay chains with observable final state* $l^+l^-\gamma + \not{E}_\top$.

see Fig. 1. Both processes lead to a final state signature of a same-flavor, opposite-sign lepton pair, one photon, and missing transverse momentum $\not{E}_\top$.

In the following we will study spin correlation effects in these decay chains in detail. We will also briefly analyze the following shorter decay modes of squarks:

$$\tilde{q}_R \to q\,\tilde{\chi}_1^0 \to q\,\gamma\,\tilde{G} \tag{2.3}$$

for GMSB, and

$$Q_-^{(1,0)} \to q\,B_\mu^{(1,0)} \to q\,\gamma\,B_H^{(1,0)} \tag{2.4}$$

for UED6. Although these decay channels have considerably larger SM backgrounds at the LHC, they also have larger branching ratios compared to the decay channels with leptons. They could be very useful to obtain information on the spin of the quark partners.

While both GMSB and UED6 have similar mass hierarchies, which allow the decay channels in eqs. (2.1)–(2.4), the typical mass spectra are quantitatively rather different.

In minimal gauge mediation the gaugino mass parameter relation $M_1/g_1^2 = M_2/g_2^2 = M_3/g_3^2$ implies that the weak gauginos are rather light, while the gluino is much heavier. Furthermore, the squarks are also heavy, while the sleptons have masses close the the gauginos. For our numerical analysis in the next section we will use the reference scenario G1a from Ref. [24]. The masses of the particles appearing in our decay chain and their branching ratios are summarized in Tab. 1.

In universal extra dimensions, on the other hand, the masses of all particles of one KK level (j,k) have the same value $m_{\rm KK}^2 = (j^2+k^2)/R^2$, where R is the size of the extra dimensions. This degeneracy is lifted only by radiative corrections [19, 23], which shift the masses by up to 20%. As a result, a typical spectrum for the particles of KK level 1 in UED6 is much less hierarchical than in GMSB. In our numerical analysis, we will use the reference scenario U1, defined by $R^{-1} = 500$ GeV, with the masses and branching ratios [20] given in Tab. 1.

These qualitative features of the spectra could be used to distinguish GMSB and UED6 experimentally. However, there are several caveats to consider: The mass spectra of GMSB can vary substantially in non-minimal models, see *e. g.* Ref. [25]. Extra dimensional models

G1a		U1	
Particle	Mass [GeV]	Particle	Mass [GeV]
$\tilde{g}$	747	$G_\mu^{(1,0)}$	696
$\tilde{u}_L$	986	$Q_+^{(1,0)}$	662
$\tilde{d}_L$	989		
$\tilde{u}_R$	942	$U_-^{(1,0)}$	608
$\tilde{d}_R$	939	$D_-^{(1,0)}$	606
$\tilde{\chi}_2^0$	224	$Z_\mu^{(1,0)}$	538
$\tilde{\chi}_1^0$	119	$B_\mu^{(1,0)}$	487
$\tilde{e}_L$	326	$L_+^{(1,0)}$	521
$\tilde{e}_R$	164	$E_-^{(1,0)}$	508
$\tilde{G}$	0	$B_H^{(1,0)}$	427
Branching ratios		Branching ratios	
$\mathrm{BR}[\tilde{g} \to q\,\bar{q}\,\tilde{\chi}_2^0]$	16%	$\mathrm{BR}[G_\mu^{(1,0)} \to q\,Q_+^{(1,0)}]$	50%
		$\mathrm{BR}[Q_+^{(1,0)} \to q\,Z_\mu^{(1,0)}]$	6.4%
$\mathrm{BR}[\tilde{\chi}_2^0 \to e^+e^-\tilde{\chi}_1^0]$	26%	$\mathrm{BR}[Z_\mu^{(1,0)} \to e^+e^-B_\mu^{(1,0)}]$	1.5%
$\mathrm{BR}[\tilde{\chi}_1^0 \to \gamma\,\tilde{G}]$	100%	$\mathrm{BR}[B_\mu^{(1,0)} \to \gamma\,B_H^{(1,0)}]$	34%

Table 1: *Masses and branching fractions for the GMSB scenario G1a (left) and the UED6 scenario U1 (right).*

are known to become strongly coupled at large energies and require some new physics to be present at the scale. The effects of this unknown high-scale physics could generate mass contributions to the KK particles in UED [26]. However, the spins of the the new particles can serve as very robust discriminators between different models.

A non-zero spin of a particle can lead to angular correlations between its decay products. At the LHC, angular correlations are manifested in the invariant mass distributions of the visible decay products of a decay chain. The long decay chains (2.1) and (2.2) are of the general form

$$D \to l_n^\pm C \to l_n^\pm l_f^\mp B \to l_n^\pm l_f^\mp \gamma A\,, \tag{2.5}$$

with $m_A < m_B < m_C < m_D$. Here we call the lepton that is emitted in the first decay step the "near-lepton" l_n, while the lepton from the second decay step is named the "far-lepton" l_f. From this one can construct the invariant masses

$$m_{n\gamma}^2 \equiv (p_{l_n} + p_\gamma)^2 = \left(m_{n\gamma}^{\max}\right)^2 \frac{1}{4}\left[2 - \left(1 - \frac{m_B^2}{m_C^2}\right)\left(1 - \cos\theta_{nf}^{(C)}\right)\right]\left(1 - \cos\theta_{n\gamma}^{(B)}\right), \tag{2.6}$$

$$m_{f\gamma}^2 \equiv (p_{l_f} + p_\gamma)^2 = \left(m_{f\gamma}^{\max}\right)^2 \frac{1}{2}\left(1 - \cos\theta_{f\gamma}^{(B)}\right), \tag{2.7}$$

$$m_{nf}^2 \equiv (p_{l_n} + p_{l_f})^2 = \left(m_{nf}^{\max}\right)^2 \frac{1}{2}\left(1 - \cos\theta_{nf}^{(C)}\right), \tag{2.8}$$

$$m_{nf\gamma}^2 \equiv (p_{l_n} + p_{l_f} + p_\gamma)^2 = m_{n\gamma}^2 + m_{f\gamma}^2 + m_{f\gamma}^2\,, \tag{2.9}$$

which are related to $\theta_{nf}^{(C)}$, the angle between the near-lepton and the far-lepton in the rest frame of C, $\theta_{n\gamma}^{(B)}$, the angle between the near-lepton and the photon in the B rest frame, and $\theta_{f\gamma}^{(B)}$, the angle between the far-lepton and the photon in the B rest frame, respectively. The maximum values for the invariant masses are given in eq. (A.2) in the appendix.

For a given decay matrix element, the distribution with respect to some invariant mass is then obtained by integrating over all remaining kinematical variables in a given reference frame, as described in detail in Refs. [7, 27].

In practice, the near and far leptons cannot be distinguished in a straightforward way. Instead the observable lepton-photon invariant mass distribution is the sum of $\mathrm{d}\Gamma/\mathrm{d}m_{n\gamma}^2 + \mathrm{d}\Gamma/\mathrm{d}m_{f\gamma}^2$. Additional information can be obtained from the distributions with respect to the minimum and maximum of the lepton-photon invariant masses,

$$m_{h\gamma}^2 = \max\{m_{n\gamma}^2, m_{f\gamma}^2\}, \qquad\qquad m_{l\gamma}^2 = \min\{m_{n\gamma}^2, m_{f\gamma}^2\}. \tag{2.10}$$

Since the total magnitude of the decay width does not carry any information about the spins of the particles involved, we will normalize the invariant mass distributions to unity,

$$\frac{1}{\Gamma_0}\frac{\mathrm{d}\Gamma}{\mathrm{d}m} \equiv \frac{\mathrm{d}P}{\mathrm{d}m}\,, \tag{2.11}$$

where Γ_0 is the integrated decay width of the given decay channel, and $\mathrm{d}P$ is defined as a differential probability density.

For the short decay chains (2.3) and (2.4) of the general form

$$C \to qB \to q\gamma A\,, \tag{2.12}$$

with $m_A < m_B < m_C$, the only observable invariant mass distribution that can be constructed is

$$m_{q\gamma}^2 \equiv (p_q + p_\gamma)^2 = \left(m_{q\gamma}^{\max}\right)^2 \frac{1}{2}\left(1 - \cos\theta_{q\gamma}^{(B)}\right). \tag{2.13}$$

Here $(m_{q\gamma}^{\max})^2 = (m_C^2 - m_B^2)(m_B^2 - m_A^2)/m_B^2$.

2.1 Spin correlations in GMSB

In GMSB the final state $l^+l^-\gamma + \not{E}_\top$ is fed by the decay chain eq. (2.1), with $\tilde{l}_{\mathrm{R}}^{\pm}$ and $\tilde{\chi}_1^0$ as intermediate particles. Since the $\tilde{l}_{\mathrm{R}}^{\pm}$ is a scalar it does not transmit any angular correlations. The fermionic $\tilde{\chi}_1^0$ can lead to non-trivial spin correlations in the decay chain, but only if the couplings at both the production and decay vertex are chiral, *i. e.* left- and right-handed components have different coupling strength [9]. While this condition is fulfilled for the $\tilde{l}_{\mathrm{R}}^{\pm}$-$l^{\mp}$-$\tilde{\chi}_1^0$ vertex, the $\tilde{\chi}_1^0$-γ-$\tilde{G}$ vertex has the form [28]

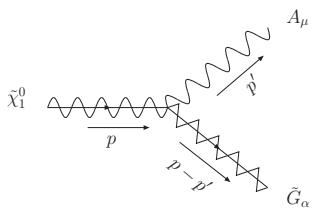

$$\propto \left[\not{p}', \gamma_\mu\right]\gamma_\alpha. \tag{2.14}$$

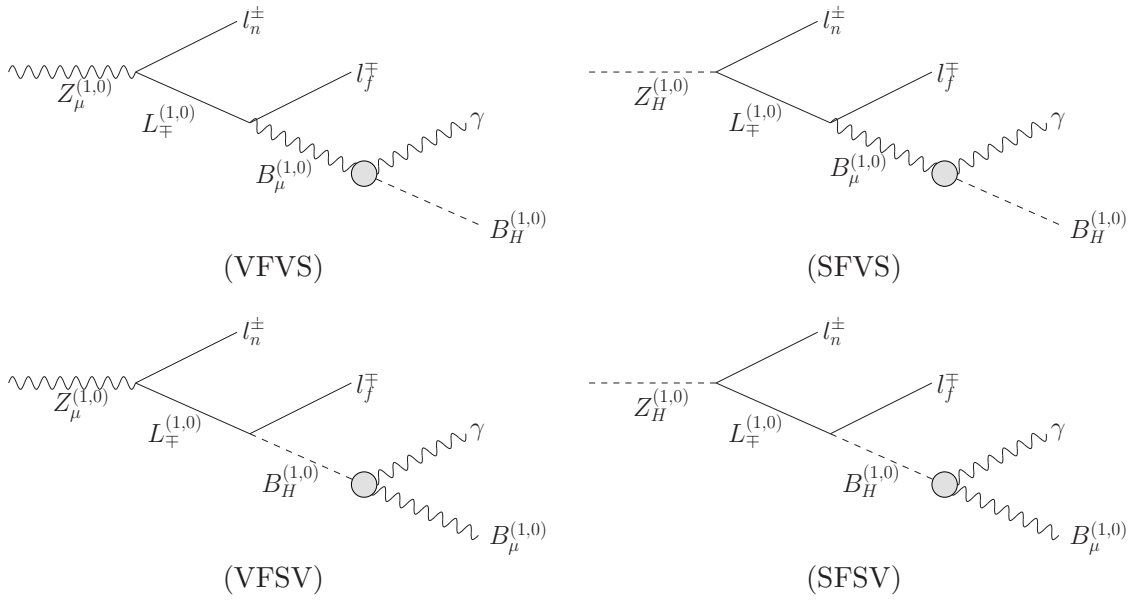

Figure 2: *Different UED6 decay chains with various spin configurations leading to the same $l^+l^-\gamma + \not{E}_\top$ signature.*

Here the left- and right-handed component of the neutralino couple with equal strength so that no observable angular correlations are generated. Thus the only features in the invariant mass distributions of the GMSB decay chain (2.1) are generated by the phase space. Analytical results for the lepton-photon and lepton-lepton distributions are listed in the appendix.

Similarly, the short decay chain eq. (2.3) does not lead to visible angular correlation effects. The quark-photon invariant mass distribution is given by

$$\frac{\mathrm{d}P}{\mathrm{d}m^2_{q\gamma}} = \frac{m_B^2}{(m_C^2 - m_B^2)(m_B^2 - m_A^2)}\,. \tag{2.15}$$

By comparison with the formulas in the appendix one can see that eq. (2.15) is identical to the $m^2_{f\gamma}$ distribution of the long chain. This can be easily understood by the fact that the chirality of the slepton and squark couplings is identical.

2.2 Spin correlations in UED6

The typical mass hierarchy generated by radiative corrections in UED6, $m_{Z_\mu^{(1,0)}} > m_{L_+^{(1,0)}} > m_{B_\mu^{(1,0)}} > m_{B_H^{(1,0)}}$, enables the decay chain eq. (2.2). However, in general sizeable corrections to the KK-particle masses could be generated by the unknown physics that complete the theory at high energies [26]. Thus for completeness we will study all possible decay chains that, for suitable mass hierarchies, could lead to the final state $l^+l^-\gamma + \not{E}_\top$, as illustrated in Fig. 2,

$$Z_\mu^{(1,0)} \to l^\pm L_\mp^{(1,0)} \to l^+l^- B_\mu^{(1,0)} \to l^+l^-\,\gamma\, B_H^{(1,0)} \qquad \text{(VFVS)}, \tag{2.16}$$

$$Z_H^{(1,0)} \to l^\pm L_\mp^{(1,0)} \to l^+l^- B_\mu^{(1,0)} \to l^+l^-\,\gamma\, B_H^{(1,0)} \qquad \text{(SFVS)}, \tag{2.17}$$

$$Z_\mu^{(1,0)} \to l^\pm L_\mp^{(1,0)} \to l^+l^- B_H^{(1,0)} \to l^+l^-\,\gamma\, B_\mu^{(1,0)} \qquad \text{(VFSV)}, \tag{2.18}$$

$$Z_H^{(1,0)} \to l^\pm L_\mp^{(1,0)} \to l^+l^- B_H^{(1,0)} \to l^+l^-\,\gamma\, B_\mu^{(1,0)} \qquad \text{(SFSV)}. \tag{2.19}$$

Here we have introduced short-hand notations for the four decay chains based on the KK particles at each decay stage being a scalar (S), fermion (F) or vector (V). Analytical results for the invariant mass distributions for all four combinations are listed in the appendix.

In case of the short decay chain, eq. (2.4), there are two possible decay chains with the same final state, depending on the mass hierarchy,

$$Q_-^{(1,0)} \to q\, B_\mu^{(1,0)} \to q\,\gamma\, B_H^{(1,0)} \qquad \text{(FVS)}, \tag{2.20}$$

$$Q_-^{(1,0)} \to q\, B_H^{(1,0)} \to q\,\gamma\, B_\mu^{(1,0)} \qquad \text{(FSV)}. \tag{2.21}$$

The quark-photon invariant mass distributions for the two cases read

FVS :

$$\frac{\mathrm{d}P}{\mathrm{d}m_{q\gamma}^2} = \frac{3m_B^4\left(2m_{q\gamma}^4 m_B^2 - 2m_{q\gamma}^2(m_A^2-m_B^2)(m_B^2-m_C^2) + (m_A^2-m_B^2)^2(m_B^2-m_C^2)\right)}{(m_A^2-m_B^2)^3(m_B^2-m_C^2)^2(2m_B^2+m_C^2)}, \tag{2.22}$$

FSV :

$$\frac{\mathrm{d}P}{\mathrm{d}m_{q\gamma}^2} = \frac{m_B^2}{(m_C^2-m_B^2)(m_B^2-m_A^2)}\,. \tag{2.23}$$

As before, one can see that these are identical to the $m_{f\gamma}^2$ distributions of the long chain for the VFVS/SFVS and VFSV/SFSV combinations, respectively. In the FSV case, since the intermediate B particle is a scalar, this decay process does not involve any spin correlations and is identical to the pure phase space distribution, and thus to the GMSB distribution.

2.3 Discussion of analytical results

Figs. 3 and 4 show the distributions for the four independent observable invariant mass combinations of the $l^+l^-\gamma+\not{E}_\top$ final state: the di-lepton invariant mass m_{nf}, the "low" and "high" lepton-invariant masses $m_{l\gamma}$ and $m_{h\gamma}$, respectively, and the lepton-lepton-photon invariant mass $m_{nf\gamma}$. Each plot contains five curves corresponding to the five models (or spin assignments) GMSB, VFVS, SFVS, VFSV, and SFSV. In case of Fig. 3, for all five models the masses have been chosen from the G1a scenario, with $m_A = m_{\tilde{G}} = 0$, $m_B = m_{\tilde{\chi}_1^0}$, $m_C = m_{\tilde{e}_R}$, and $m_D = m_{\tilde{\chi}_2^0}$. On the other hand, Fig. 4 shows the situation for the U1 spectrum with $m_A = m_{B_H}$, $m_B = m_{B_\mu}$, $m_C = m_{L_+}$, and $m_D = m_{Z_\mu}$.

As evident from the plots, different distributions could discriminate between different spin assignments. The di-lepton distribution $\mathrm{d}P/\mathrm{d}m_{nf}$ is markedly different for the VFSV and SFSV models, where the B particle is a scalar, compared to the other models. This can be understood from the fact that the chiral structure of the KK-fermion couplings to

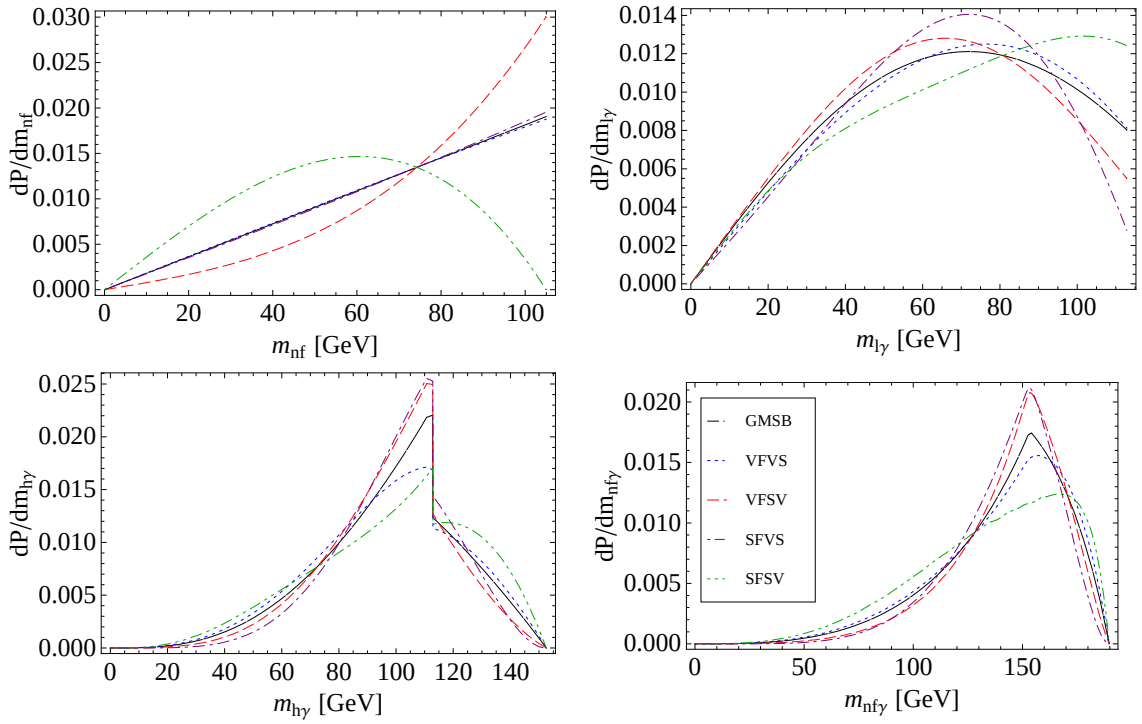

Figure 3: *Observable invariant mass distributions for the decay chain in eq.* (2.5) *for different models and masses from the G1a scenario.*

KK-scalars or KK-vector bosons is different (see for example Ref. [10] for more details). On the other hand, the peak in the $\mathrm{d}P/\mathrm{d}m_{h\gamma}$ and $\mathrm{d}P/\mathrm{d}m_{nf\gamma}$ spectra is relatively enhanced for the VFSV and SFVS models. As a result, the discriminative power between different spin assignments is maximized by including all four distributions in the analysis.

Fig. 5 shows the jet-photon invariant mass distribution for the short decay chain. For the distribution on the left hand side the masses have been chosen from the G1a scenario, $m_A = m_{\tilde{G}} = 0$, $m_B = m_{\tilde{\chi}_1^0}$, $m_C = m_{\tilde{u}_R}$ and on the right hand side the distribution is shown for the U1 scenario, where $m_A = m_{B_H^{(1,0)}}$, $m_B = m_{B_\mu^{(1,0)}}$, $m_C = m_{Q_-^{(1,0)}}$. As mentioned before, the GMSB and FSV chains both do not generate any spin correlations and thus cannot be distinguished from each other. However, the plots show a discrimination potential between FVS and the other two cases, especially for the G1a mass scenario. The qualitative features of the jet-photon distribution are similar for the G1a and U1 scenarios, although the spin correlation effects are less pronounced for the more degenerate U1 mass spectrum than for the more hierarchical G1a spectrum.

3. Monte-Carlo simulation and numerical analysis

In the previous section theoretical formulas for the invariant mass spectra of decay chains in GMSB and UED6 were discussed. However, in a realistic experimental setup one must take into account several effects that influence the measured distributions.

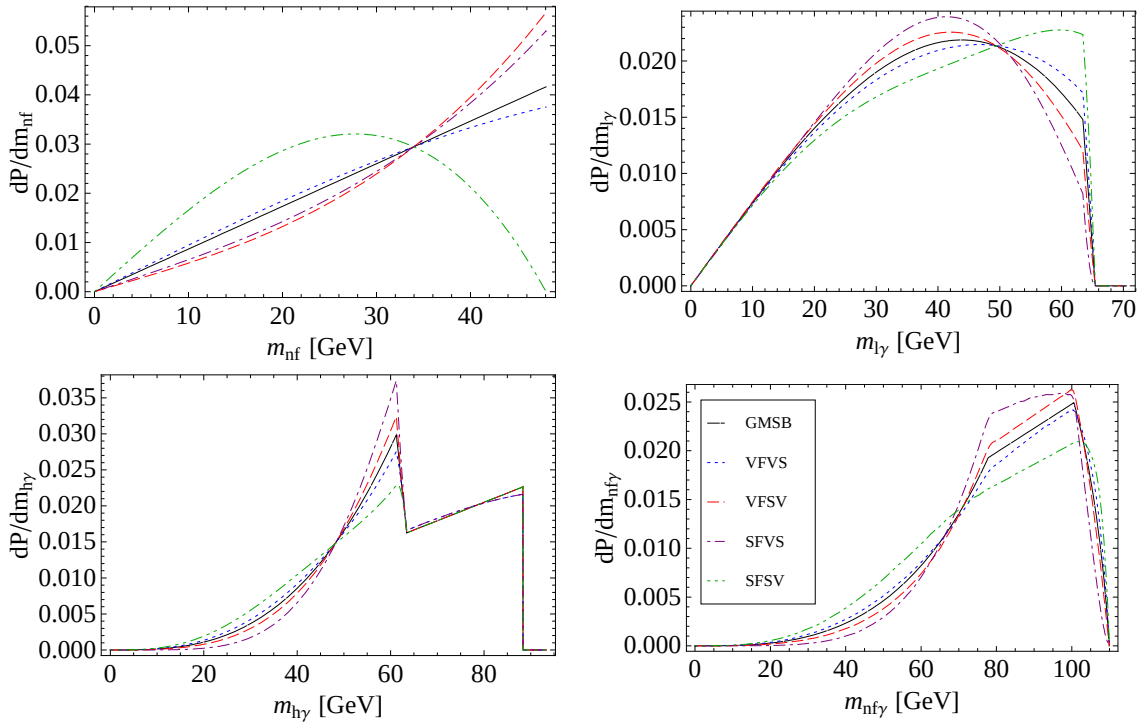

Figure 4: *Observable invariant mass distributions for the decay chain in eq.* (2.5) *for different models and masses from the U1 scenario.*

- Detector effects, such as limited resolution, and reconstruction effects from particle identification can smear out the visible invariant mass distributions. Further, detector acceptance can distort the shape of the distribution.

- For the separation of the new physics signal from the SM backgrounds suitable selection cuts have to be implemented, which can distort the shape of the distributions.

- Since both SUSY and KK particles are produced in pairs, often there will be two

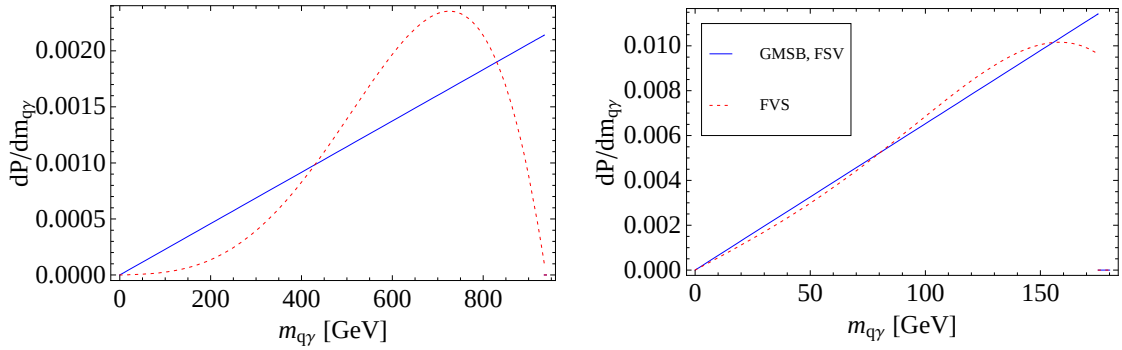

Figure 5: *Observable invariant mass distributions for the short decay chain in eq.* (2.12) *for masses from the G1a scenario (left) and U1 scenario (right).*

hard photons in one event, leading to a two-fold ambiguity in the reconstruction of the correct decay chain.

Therefore we have performed a realistic experimental simulation of the new physics signal from the long decay chain for GMSB and UED6, with the goal of reconstructing the spin-sensitive invariant mass distributions and discriminating between models from the simulated data.

The decay chains in eqs. (2.1), (2.16)–(2.19) have been computed with CompHEP 4.4 [29] for 14 TeV proton-proton collisions, using the GMSB model file from Ref. [30] and our own implementation of the UED6 model. Parton-level events generated with CompHEP were then passed on to Pythia 6.4.12 [31]. Finally, the ATLAS detector[32] is simulated using the parametrized fast detector simulation ATLFAST[33, 34], which includes detector acceptance, resolution and some basic particle identification.

For the G1a and U1 mass spectra, the aforementioned decay chains are initiated mostly by squark (KK-quark) and gluino (KK-gluon) production processes, respectively. Since our analysis does not depend crucially on the details of the hadronic decay products of the squarks (KK-quarks) and gluinos (KK-gluons) we have only generated events for squark (KK-quark) pair production as the primary hard process, and then normalized the total event count according to the total production cross section including gluino (KK-gluon) processes.

As a further simplification, we have only generated matrix elements with the decay chain of one of the two squarks (KK-quarks) within CompHEP, which correctly implements all spin correlations. The decay of the second squark (KK-quark) was simulated in Pythia, without spin correlations. Nevertheless, this procedure provides a good approximation to the complete matrix elements since the branching ratio for the decay chain leading to the final state $l^+l^-\gamma$ is relatively small and thus only a very small fraction of the events contains two decay cascades of this type. Moreover, Pythia was used for simulating initial and final state radiation and hadronization.

The event selection was performed according to Ref. [24]. First the effective mass

$$M_{\text{eff}} = \not{E}_\top + p_{\top,1} + p_{\top,2} + p_{\top,3} + p_{\top,4} \tag{3.1}$$

is defined, where $\not{E}_\top$ denotes the missing transverse energy and $p_{\top,i}$ the transverse momenta of the 4 hardest jets. The selected events need to fulfill the following conditions:

1. 4 jets with transverse momenta > 25 GeV,
2. $M_{\text{eff}} > 400$ GeV,
3. $\not{E}_\top > 0.1\, M_{\text{eff}}$,
4. 2 photons with transverse momenta > 20 GeV,
5. 2 electrons or muons with transverse momenta > 20 GeV.

After application of these cuts the SM background is reduced to a negligible level [24], while about 20% of the signal is retained.

Since the selected events include two photons, one of them has to be selected to compute the invariant mass distributions. Good results are obtained, when choosing the one photon, which gives the smaller $m^2_{nf\gamma}$ invariant mass.

It would be interesting to also analyze the short decay chain in a complete simulation, since the expected rates are large (about 5 pb both for G1a and U1). However, the signature of this final state, two hard jets, two photons, and missing energy, is very sensitive to issues related to jets faking photons. Therefore, it would require a more careful analysis of QCD backgrounds, which will be left for a future publication.

3.1 Cross Sections

For a realistic analysis, the model-dependent cross-sections and event numbers have to be calculated. At the G1a point, the total squark and gluino production cross section is $\sigma_{\tilde{q}/\tilde{g}} = 7.6$ pb [24]. Since the gluino is lighter than the squarks, the squarks decay through cascades involving a gluino. With the branching ratios from Tab. 1 a good approximation for the cross section for the decay chain is

$$\begin{aligned}\sigma_{\mathrm{G1a}} &= \sigma_{\tilde{q}/\tilde{g}} \times 2 \times 2 \times \mathrm{BR}\left[\tilde{g} \to q\bar{q}\tilde{\chi}_2^0\right] \times \mathrm{BR}\left[\tilde{\chi}_2^0 \to e^+e^-\tilde{\chi}_1^0\right] \times \mathrm{BR}\left[\tilde{\chi}_1^0 \to \gamma\tilde{G}\right] \\ &\simeq 1.2 \text{ pb}. \end{aligned} \tag{3.2}$$

The factors of 2 result from the two generations of leptons in the di-leptonic decay chain and the fact that squarks or gluinos are produced in pairs and both of them can decay through this channel.

In the U1 model, the KK-quarks and KK-gluons are produced with the following cross sections [20]

$$\begin{aligned} &\sigma_{Q_+^{(1,0)}Q_+^{(1,0)}} \sim 7 \text{ pb}, && \sigma_{Q_+^{(1,0)}Q_-^{(1,0)}} \sim 18 \text{ pb}, \\ &\sigma_{G_\mu^{(1,0)}G_\mu^{(1,0)}} \sim 10 \text{ pb}, && \sigma_{G_\mu^{(1,0)}Q_+^{(1,0)}} \sim 24 \text{ pb}, \\ &\sigma_{G_\mu^{(1,0)}Q_-^{(1,0)}} \sim 26 \text{ pb}. \end{aligned} \tag{3.3}$$

In this scenario, KK-quarks are lighter than the KK-gluon, such that the latter will mostly decay into KK-quarks. Therewith, the total KK-quark production cross section is

$$\begin{aligned}\sigma_{Q_+^{(1,0)}} &= 2\,\sigma_{Q_+^{(1,0)}Q_+^{(1,0)}} + \sigma_{Q_+^{(1,0)}Q_-^{(1,0)}} + 2\,\mathrm{BR}\left[G_\mu^{(1,0)} \to Q_+^{(1,0)}q\right]\sigma_{G_\mu^{(1,0)}G_\mu^{(1,0)}} \\ &\quad + \left(1 + \mathrm{BR}\left[G_\mu^{(1,0)} \to Q_+^{(1,0)}q\right]\right)\,\sigma_{G_\mu^{(1,0)}Q_+^{(1,0)}} + \mathrm{BR}\left[G_\mu^{(1,0)} \to Q_+^{(1,0)}q\right]\,\sigma_{G_\mu^{(1,0)}Q_-^{(1,0)}}. \end{aligned} \tag{3.4}$$

As above, factors of 2 account for the two sides of the pair production process. Then the total cross section for the decay chain adds up to

$$\begin{aligned}\sigma_{\mathrm{U1}} &= \sigma_{Q_+^{(1,0)}} \times 2 \times 2 \times \mathrm{BR}\left[Q_+^{(1,0)} \to qZ_\mu^{(1,0)}\right] \times \mathrm{BR}\left[Z_\mu^{(1,0)} \to e^+e^-B_\mu^{(1,0)}\right] \\ &\quad \times \mathrm{BR}\left[B_\mu^{(1,0)} \to \gamma B_H^{(1,0)}\right] \simeq 0.12 \text{ pb}. \end{aligned} \tag{3.5}$$

	GMSB	VFVS	VFSV	SFVS	SFSV
GMSB		0.000 ($m_{h\gamma}$)	0.000 (m_{nf})	0.006 ($m_{h\gamma}$)	0.000 (m_{nf})
VFVS	0.056 ($m_{h\gamma}$)		0.000 (m_{nf})	0.000 ($m_{h\gamma}$)	0.000 (m_{nf})
VFSV	0.577 (m_{nf})	0.155 ($m_{h\gamma}$)		0.000 (m_{nf})	0.000 (m_{nf})
SFVS	0.025 ($m_{l\gamma}$)	0.065 ($m_{l\gamma}$)	0.084 ($m_{h\gamma}$)		0.000 (m_{nf})
SFSV	0.000 (m_{nf})	0.000 (m_{nf})	0.000 (m_{nf})	0.000 (m_{nf})	

Table 2: *Minimal χ^2-probabilities for 10 fb^{-1}. The distributions that provide the strongest constraints are noted in parentheses. The values in the blue cells (upper right) are for the G1a mass spectrum and in the red cells (lower left) are the values for the U1 mass spectrum.*

Using the signal efficiency of the cuts in Ref. [24] and assuming an integrated luminosity of 10 fb^{-1} we obtain $N^{(10)}_{G1a} = 2500$ selected events for the G1a point and $N^{(10)}_{U1} = 250$ selected events for the U1 model.

It should be noted that the event rates depend strongly on the underlying model and its parameters, as well as the choice of selection cuts. Furthermore, the signal efficiency after cuts depends also on the decay chain of the second squark or KK-quark, whose branching ratios vary between different models. For the purpose of this study, we do not vary the choice of cuts, cross sections and signal efficiency between different models when we compare them for one given mass spectrum (i. e. for all spin assignments we assume 2500 selected events for the G1a mass spectrum and 250 selected events for the U1 mass spectrum). Rather, our numerical analysis of the two scenarios should only serve as concrete examples for a spin determination of a new physics signal, in particular since our method does not rely on information about total rates.

3.2 χ^2 Analysis

In order to discriminate the histograms for the different spin configurations we used the χ^2-test implemented in ROOT [35]. It returns the χ^2-probability, i. e. the probability that two histograms with identical underlying distribution functions have a bigger χ^2 value than the two compared ones. Since these values depend on the number of bins, the discrimination was performed with 5 bins, which showed the best discriminative power at 10 fb^{-1}. In Tab. 2 the minimal χ^2 probabilities for each pair of spin configurations are listed.

The results of the χ^2 probabilities reflect the general features that can be seen in the histograms of Fig. 6 and 7. As expected, the discrimination between different spin combinations is far more effective for the G1a scenario than for the U1 scenario, as a result of the more degenerate mass spectrum and lower cross section in the latter case. For the G1a scenario, even with 10 fb^{-1} almost all models can be distinguished with a confidence level better than 99.9%. In the case of the U1 scenario only the SFSV spin assignment can be distinguished at this confidence level with 10 fb^{-1} luminosity, owing to the distinctly different shape of the distribution of the di-lepton invariant mass m_{nf}. In other cases however, in particular for the GMSB spin assignment and the extra-dimensional chain VFSV, it is not possible to make a distinction even at the 95% confidence level. Here a much larger integrated luminosity would be required for a significant discrimination.

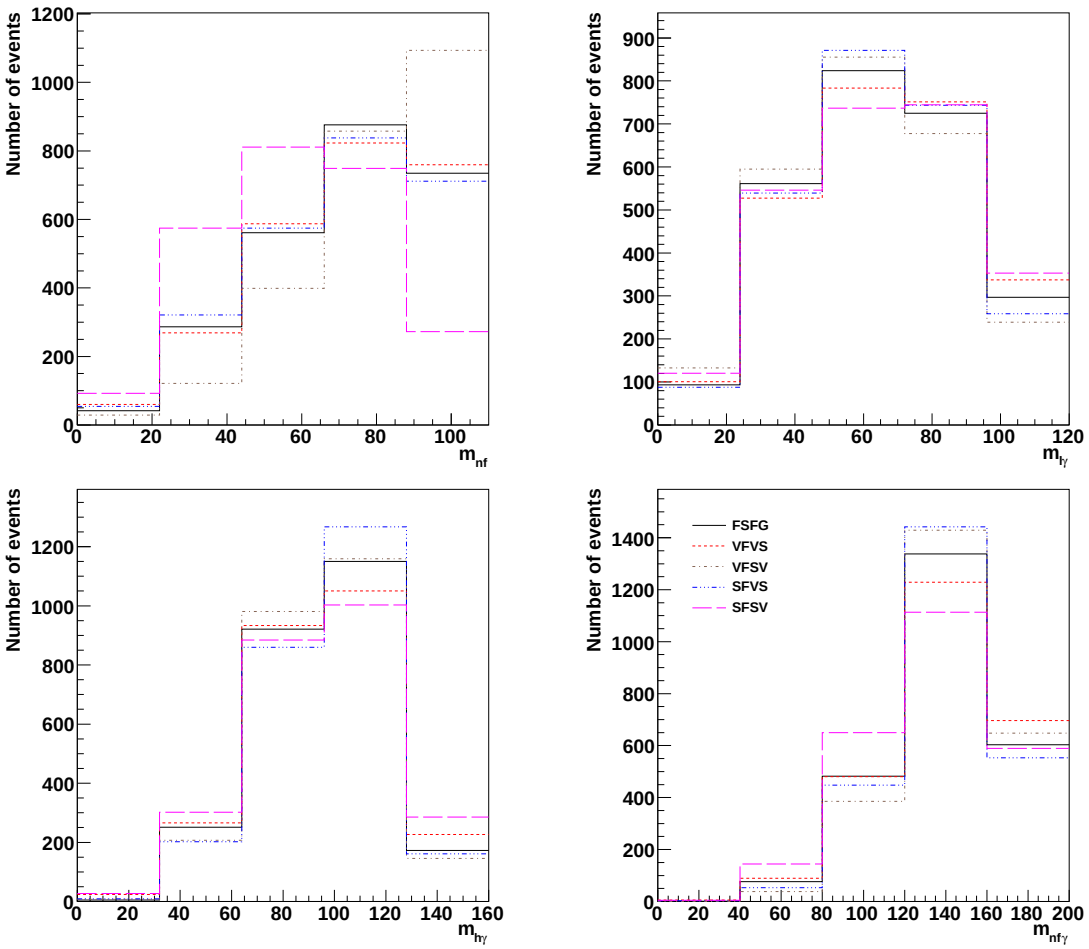

Figure 6: *Reconstructed invariant mass distribution from ATLFAST detector simulation, corresponding to G1a masses and cross sections for 10 fb^{-1} integrated luminosity. The histograms have been divided into 5 bins.*

As an example Fig. 8 shows the reconstructed invariant mass distributions corresponding to G1a masses for an integrated luminosity of 30 fb^{-1}. The distributions are divided in 10 bins, which gives the best discriminative power for this luminosity. More shape information is available due to more bins and events allowing for a better separation between the different models. For the U1 mass scenario the GMSB spin assignment can be distinguish from the extra-dimensional chain VFSV at almost 90% confidence level.

Nevertheless, in summary the analysis of invariant mass distributions proves to be a powerful tool to identify the spins of particles in decay chains with hard photons.

4. Conclusion

In this article we have analyzed the prospects for determining the spins of new particles in decay chains with photons and missing energy at the LHC. As concrete model incarnations of such signatures we considered supersymmetry with gauge-mediated breaking (GMSB)

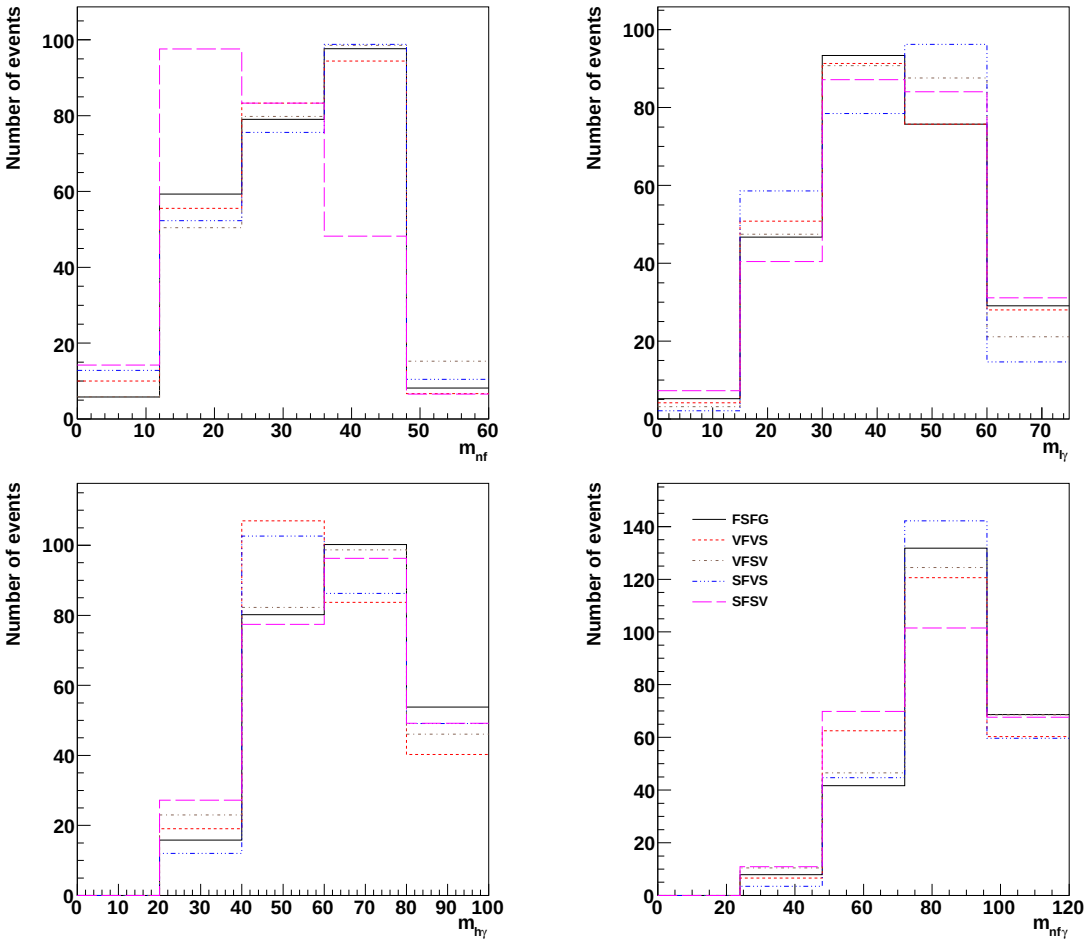

Figure 7: *Same as Fig. 6, but for U1 masses and cross sections.*

and the standard model with two universal extra dimensions (UED6). Each of these models predicts new partners of the SM particles, the lightest of which is stable on grounds of a conserved parity. The supersymmetric or KK partner of the photon can decay into this stable particle and a hard photon. At the LHC the partners of the colored particles (squarks/gluinos or KK-quarks/KK-gluons) are produced with large cross sections and subsequently could decay in several steps until the final photon emission step. As became well known in recent years, the distributions of the invariant masses of two or more of the decay products is sensitive to the spins of the decaying particles. The measurement of the spins of the new particles is of central interest since this is the crucial difference between supersymmetry and extra dimensions.

Following this approach, we first derived analytical expressions for the invariant mass distributions for characteristic decay chains of those two models. In greater detail we analyzed a class of decay chains that lead to two leptons, one photon, and missing energy. This signature can stem from five different decay processes (one in GMSB, four in UED6), which differ by the spins of the intermediate particles. It was found that different invariant

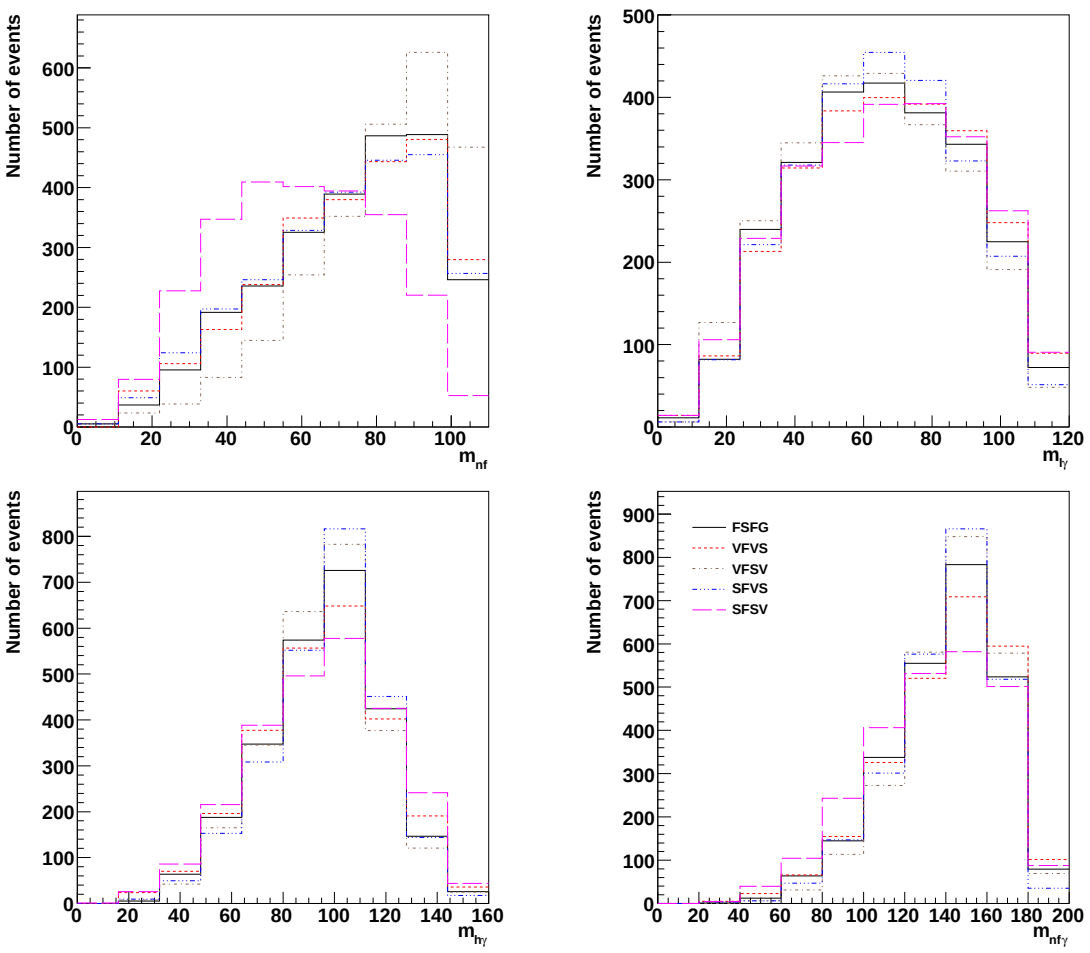

Figure 8: *Reconstructed invariant mass distribution from ATLFAST detector simulation, corresponding to G1a masses and cross sections for 30 fb^{-1} integrated luminosity. The histograms have been divided into 10 bins.*

mass distributions show different distinctive features between those five cases, so that the discriminative power is maximized by combining information from all distributions. In a second step, we performed a realistic phenomenological Monte-Carlo analysis including a fast detector simulation for those five processes. Due to detector effects and cuts for background rejection, the reconstructed invariant mass distributions are distorted compared to the analytical parton-level results. Nevertheless, the essential characteristic features of the five different spin assignments are preserved, so that the spins of the intermediate particles can be determined.

For a typical GMSB mass spectrum with superpartner masses below 1 TeV, we found that with 10 fb^{-1} integrated luminosity almost all of the five different spin assignments, and in particular the GSMB and UED6 models, can be distinguished with 99.9% confidence level. A typical UED6 spectrum, on the other hand, is more degenerate, leading to smaller branching ratios to leptons and to suppressed spin correlation effects in the invariant mass distributions. As a result, for such a mass spectrum, GMSB and UED6 can only be distin-

guished with a confidence level of less than 50% with 10 fb^{-1}. A much higher luminosity would be needed for better discrimination in this scenario.

Additional information could be obtained by looking at other decay chains. We briefly investigated decay chains leading to a hard jet, a photon, and missing energy, but no leptons. Such a decay chain has a large branching fraction for UED6 scenarios and thus might be useful for discriminating models in this case. A more conclusive answer would require a detailed analysis of backgrounds to this process, which is beyond the scope of this work.

In summary, it appears feasible to distinguish GMSB and six-dimensional UED models with LHC data alone if the mass spectrum is not very degenerate.

Acknowledgments

This work was supported in part by the Schweizer Nationalfonds. A. F. is grateful for warm hospitality at the Universität Zürich, Argonne National Laboratory and the University of Chicago, where part of this work was performed. W. E. is grateful for warm hospitality at the Universität Zürich, where part of this work was performed.

We thank members of the ATLAS Collaboration for helpful discussions. We have made use of the ATLAS physics analysis framework and tools which are the result of collaboration-wide efforts.

A. Analytical results for invariant mass distributions

In the appendix we list analytical results for the invariant mass distributions of the various GMSB and UED6 decay chains discussed in section 2. All those decay chains are of the form

$$D \to l_n^{\pm} C \to l_n^{\pm} l_f^{\mp} B \to l_n^{\pm} l_f^{\mp} \gamma A \,, \tag{A.1}$$

with $m_A < m_B < m_C < m_D$. Owing to kinematical constraints, the invariant mass distributions are divided into sections, which are bounded by the kinematical edges

$$\begin{aligned}
(m_{f\gamma}^{\max})^2 &= \frac{(m_C^2 - m_B^2)(m_B^2 - m_A^2)}{m_B^2}, \\
(m_{n\gamma}^{\max})^2 &= \frac{(m_D^2 - m_C^2)(m_B^2 - m_A^2)}{m_B^2}, \\
(m_{No}^{\max})^2 &= \frac{(m_D^2 - m_C^2)(m_C^2 - m_B^2)}{m_C^2}, \\
(m_{n2}^{\max})^2 &= \frac{(m_D^2 - m_C^2)(m_B^2 - m_A^2)}{2m_C^2 - m_D^2}.
\end{aligned} \tag{A.2}$$

Therefore the distributions take on the following structures:

The far-lepton–photon mass distribution $\frac{\mathrm{d}P}{\mathrm{d}m_{f\gamma}^2}$:

$$\frac{\mathrm{d}P}{\mathrm{d}m_{f\gamma}^2} = C 1_f. \tag{A.3}$$

The near-lepton–photon mass distribution $\frac{\mathbf{d}P}{\mathbf{d}m^2_{n\gamma}}$:

$$\frac{\mathrm{d}P}{\mathrm{d}m^2_{n\gamma}} = \begin{cases} C1_n\,, & 0 \le m \le m^{\max}_{n\gamma}\frac{m_B}{m_C} \\ C2_n\,, & m^{\max}_{n\gamma}\frac{m_B}{m_C} < m \le m^{\max}_{n\gamma}. \end{cases} \tag{A.4}$$

The high lepton–photon mass distribution $\frac{\mathbf{d}P}{\mathbf{d}m^2_{h\gamma}}$:

Hierarchy A11: $m^{\max}_{f\gamma} < m^{\max}_{n\gamma}\frac{m_B}{m_C} < m^{\max}_{n\gamma} < m^{\max}_{n2}$

$$\frac{\mathrm{d}P}{\mathrm{d}m^2_{h\gamma}} = \begin{cases} C1_{hA11}\,, & 0 \le m \le m^{\max}_{f\gamma} \\ C2_{hA11}\,, & m^{\max}_{f\gamma} < m \le m^{\max}_{n\gamma}\frac{m_B}{m_C} \\ C3_{hA11}\,, & m^{\max}_{n\gamma}\frac{m_B}{m_C} < m \le m^{\max}_{n2}. \end{cases} \tag{A.5}$$

Hierarchy A12: $m^{\max}_{n\gamma}\frac{m_B}{m_C} < m^{\max}_{f\gamma} < m^{\max}_{n\gamma} < m^{\max}_{n2}$

$$\frac{\mathrm{d}P}{\mathrm{d}m^2_{h\gamma}} = \begin{cases} C1_{hA12}\,, & 0 \le m \le m^{\max}_{n\gamma}\frac{m_B}{m_C} \\ C2_{hA12}\,, & m^{\max}_{n\gamma}\frac{m_B}{m_C} < m \le m^{\max}_{f\gamma} \\ C3_{hA12}\,, & m^{\max}_{f\gamma} < m \le m^{\max}_{n2}. \end{cases} \tag{A.6}$$

Hierarchy A2: $m^{\max}_{n\gamma}\frac{mB}{mC} > m^{\max}_{n2} > m^{\max}_{n\gamma} > m^{\max}_{f\gamma}$

$$\frac{\mathrm{d}P}{\mathrm{d}m^2_{h\gamma}} = \begin{cases} C1_{hA2}\,, & 0 \le m \le m^{\max}_{n\gamma}\frac{m_B}{m_C} \\ C2_{hA2}\,, & m^{\max}_{n\gamma}\frac{m_B}{m_C} < m \le m^{\max}_{n2} \\ C3_{hA2}\,, & m^{\max}_{n2} < m \le m^{\max}_{f\gamma}. \end{cases} \tag{A.7}$$

Hierarchy B1: $m^{\max}_{f\gamma} < m^{\max}_{n\gamma}\frac{m_B}{m_C} < m^{\max}_{n\gamma}$

$$\frac{\mathrm{d}P}{\mathrm{d}m^2_{h\gamma}} = \begin{cases} C1_{hB1}\,, & 0 \le m \le m^{\max}_{f\gamma} \\ C2_{hB1}\,, & m^{\max}_{f\gamma} < m \le m^{\max}_{n\gamma}\frac{m_B}{m_C} \\ C3_{hB1}\,, & m^{\max}_{n\gamma}\frac{m_B}{m_C} < m \le m^{\max}_{n\gamma}. \end{cases} \tag{A.8}$$

Hierarchy B2: $m^{\max}_{n\gamma}\frac{m_B}{m_C} < m^{\max}_{f\gamma} < m^{\max}_{n\gamma}$

$$\frac{\mathrm{d}P}{\mathrm{d}m^2_{h\gamma}} = \begin{cases} C1_{hB2}\,, & 0 \le m \le m^{\max}_{n\gamma}\frac{m_B}{m_C} \\ C2_{hB2}\,, & m^{\max}_{n\gamma}\frac{m_B}{m_C} < m \le m^{\max}_{f\gamma} \\ C3_{hB2}\,, & m^{\max}_{f\gamma} < m \le m^{\max}_{n\gamma}. \end{cases} \tag{A.9}$$

The low lepton-photon mass distribution $\frac{\mathbf{d}P}{\mathbf{d}m^2_{l\gamma}}$:

Hierarchy A1: $m^{\max}_{f\gamma} < m^{\max}_{n\gamma} < m^{\max}_{n2}$

$$\frac{\mathrm{d}P}{\mathrm{d}m^2_{l\gamma}} = C1_{lA1} \tag{A.10}$$

Hierarchy A2: $m_{n2}^{\max} < m_{n\gamma}^{\max} < m_{f\gamma}^{\max}$

$$\frac{\mathrm{d}P}{\mathrm{d}m_{l\gamma}^2} = \begin{cases} C1_{lA2}\,, & 0 \le m \le m_{n2}^{\max} \\ C2_{lA2}\,, & m_{n2}^{\max} < m \le m_{n\gamma}^{\max}. \end{cases} \tag{A.11}$$

Hierarchy B: $m_{f\gamma}^{\max} < m_{n\gamma}^{\max}$

$$\frac{\mathrm{d}P}{\mathrm{d}m_{l\gamma}^2} = C1_{lB}. \tag{A.12}$$

Many of these coefficients are related:

$$\begin{aligned} &C1_f = C3_{A2}, \\ &C1_n = C2_{hA11} = C2_{hB1}, \\ &C2_n = C3_{hA11} = C3_{hA12} = C3_{hB1} = C3_{hB2} = C2_{lA2}, \\ &C1_{hA11} = C1_{hA12} = C1_{hA2} = C1_{hB1} = C1_{hB2}, \\ &C2_{hA12} = C2_{hA2} = C2_{hB2}, \\ &C1_{lA1} = C1_{lA2} = C1_{lB}. \end{aligned} \tag{A.13}$$

Below the results for the independent coefficients are given:

GMSB = phase space:

$$C1_f = \frac{m_B^2}{\left(m_A^2 - m_B^2\right)\left(m_B^2 - m_C^2\right)}\,, \tag{A.14}$$

$$C1_n = \frac{m_B^2 m_C^2 \log\left[\frac{m_B^2}{m_C^2}\right]}{\left(m_A^2 - m_B^2\right)\left(m_B^2 - m_C^2\right)\left(m_C^2 - m_D^2\right)}\,, \tag{A.15}$$

$$C2_n = \frac{m_B^2 m_C^2 \log\left[\frac{m^2 m_B^2}{\left(m_A^2 - m_B^2\right)\left(m_C^2 - m_D^2\right)}\right]}{\left(m_A^2 - m_B^2\right)\left(m_B^2 - m_C^2\right)\left(m_C^2 - m_D^2\right)}\,, \tag{A.16}$$

$$C1_{hA11} = -\frac{m_B^2 m_C^2 \left(m^2 + 2\left(m^2 - m_A^2 + m_B^2\right)\operatorname{arccoth}\left[\frac{m^2 - 2m_A^2 + 2m_B^2}{m^2}\right]\right)}{\left(m_A^2 - m_B^2\right)\left(m^2 - m_A^2 + m_B^2\right)\left(m_B^2 - m_C^2\right)\left(m_C^2 - m_D^2\right)}\,, \tag{A.17}$$

$$C2_{hA12} = -\frac{m_B^2 m_C^2 \left(m^2 + \left(m^2 - m_A^2 + m_B^2\right)\log\left[-\frac{\left(m^2 - m_A^2 + m_B^2\right)\left(m_C^2 - m_D^2\right)}{m^2 m_C^2}\right]\right)}{\left(m_A^2 - m_B^2\right)\left(m^2 - m_A^2 + m_B^2\right)\left(m_B^2 - m_C^2\right)\left(m_C^2 - m_D^2\right)}\,, \tag{A.18}$$

$$\begin{aligned} C1_{lA1} = \Bigg(& m_B^2 m_C^2 \Bigg(2m^2 - m_A^2 + m_B^2 - \frac{(m^2 - m_A^2 + m_B^2) m_D^2}{m_C^2} \\ & + (m^2 - m_A^2 + m_B^2) \log\left[\frac{m_B^2 (m^2 - m_A^2 + m_B^2)}{(-m_A^2 + m_B^2) m_C^2}\right] \Bigg) \Bigg) \\ & \Big/ \Big((m_A^2 - m_B^2)(m^2 - m_A^2 + m_B^2)(m_B^2 - m_C^2)(m_C^2 - m_D^2) \Big)\,. \end{aligned} \tag{A.19}$$

VFVS:

$$C1_f = \Big(3m_B^4(2m^4m_B^2 - 2m^2(m_A^2 - m_B^2)(m_B^2 - m_C^2) + (m_A^2 - m_B^2)^2 \times (m_B^2 - m_C^2))\Big)/\Big((m_A^2 - m_B^2)^3(m_B^2 - m_C^2)^2(2m_B^2 + m_C^2)\Big), \tag{A.20}$$

$$\begin{aligned} C1_n = \Big(&6m_B^2m_C^2((m_B^2 - m_C^2)(4m^2m_B^2m_C^2(m_C^2 - 2m_D^2) \\ &+ (m_A^2 - m_B^2)(m_C^2 - m_D^2)(m_B^2m_C^2 - 2(2m_B^2 + m_C^2)m_D^2)) \\ &- 2m_B^2(2m^2m_C^2(m_B^2 + m_C^2)(m_C^2 - 2m_D^2) \\ &+ (m_A^2 - m_B^2)(m_C^2 - m_D^2)(m_C^4 - 2(m_B^2 + 2m_C^2)m_D^2))\log\left[\frac{m_B}{m_C}\right])\Big) \\ &/\Big((m_A^2 - m_B^2)^2(m_B^2 - m_C^2)^2(2m_B^2 + m_C^2)(m_C^2 - m_D^2)^2(m_C^2 + 2m_D^2)\Big), \end{aligned} \tag{A.21}$$

$$\begin{aligned} C2_n = \Bigg(&6m_B^2m_C^2\Bigg(m_C^2(2m^4m_B^4m_C^2 - (m_A^2 - m_B^2)^2(m_C^2 - m_D^2) \\ &\times (3m_B^2m_C^2 - 2(5m_B^2 + m_C^2)m_D^2) + m^2m_B^2(m_A^2 - m_B^2) \\ &\times (-2m_C^4 + m_B^2(3m_C^2 - 10m_D^2))) + m_B^2(m_A^2 - m_B^2)(2m^2m_C^2(m_B^2 + m_C^2) \\ &\times (m_C^2 - 2m_D^2) + (m_A^2 - m_B^2)(m_C^2 - m_D^2)(m_C^4 - 2(m_B^2 + 2m_C^2)m_D^2)) \\ &\times \log\left[\frac{(m_A^2 - m_B^2)(m_C^2 - m_D^2)}{m^2m_B^2}\right]\Bigg)\Bigg) \\ &/\Big((m_A^2 - m_B^2)^3(m_B^2 - m_C^2)^2(2m_B^2 + m_C^2)(m_C^2 - m_D^2)^2(m_C^2 + 2m_D^2)\Big), \end{aligned} \tag{A.22}$$

$$\begin{aligned} C1_{hA11} = \Bigg(&3m_B^4m_C^2\Bigg(m^2(-2(m_A^2 - m_B^2)^4(m_C^2 - m_D^2) \\ &\times (m_C^4 + 2m_B^2m_D^2 - 8m_C^2m_D^2) + 6m^8m_B^2(m_C^4 - 4m_C^2m_D^2 + 2m_D^4) \\ &- 2m^6(m_A^2 - m_B^2)(m_C^6 + 6m_C^4m_D^2 - 8m_C^2m_D^4 \\ &+ 9m_B^2(m_C^4 - 4m_C^2m_D^2 + 2m_D^4)) + m^4(m_A^2 - m_B^2)^2 \\ &\times (5m_C^6 + 34m_C^4m_D^2 - 44m_C^2m_D^4 + m_B^2(19m_C^4 - 78m_C^2m_D^2 + 40m_D^4)) \\ &- m^2(m_A^2 - m_B^2)^3(m_B^2(7m_C^4 - 34m_C^2m_D^2 + 20m_D^4) \\ &- m_C^2(m_C^4 - 44m_C^2m_D^2 + 44m_D^4))) - 2(m_A^2 - m_B^2)(m^2 - m_A^2 + m_B^2)^3 \\ &\times (2m^2m_C^2(m_B^2 + m_C^2)(m_C^2 - 2m_D^2) + (m_A^2 - m_B^2)(m_C^2 - m_D^2) \\ &\times (m_C^4 - 2(m_B^2 + 2m_C^2)m_D^2))\log\left[1 - \frac{m^2}{m^2 - m_A^2 + m_B^2}\right]\Bigg)\Bigg) \\ &/\Big((m_A^2 - m_B^2)^3(m^2 - m_A^2 + m_B^2)^3(m_B^2 - m_C^2)^2 \\ &\times (2m_B^2 + m_C^2)(m_C^2 - m_D^2)^2(m_C^2 + 2m_D^2)\Big), \end{aligned} \tag{A.23}$$

$$
\begin{aligned}
C2_{hA12} = \Bigg(& 3m_B^4 m_C^2 \Bigg(\frac{1}{(m^2 - m_A^2 + m_B^2)^3} (2(m_A^2 - m_B^2)^5 (m_B^2 + 2m_C^2) \\
& \times (m_C^4 - 5m_C^2 m_D^2 + 4m_D^4) + 2m^{10} m_B^2 (5m_C^4 - 12m_C^2 m_D^2 + 6m_D^4) \\
& - m^4 (m_A^2 - m_B^2)^3 (-25m_C^6 + 152m_C^4 m_D^2 - 92m_C^2 m_D^4 \\
& + m_B^2 (11m_C^4 + 8m_C^2 m_D^2 - 4m_D^4)) - 2m^8 (m_A^2 - m_B^2) \\
& \times (-m_C^2 (m_C^4 - 14m_C^2 m_D^2 + 8m_D^4) + 2m_B^2 (8m_C^4 - 17m_C^2 m_D^2 + 9m_D^4)) \\
& - 2m^2 (m_A^2 - m_B^2)^4 (9m_C^6 - 47m_C^4 m_D^2 + 32m_C^2 m_D^4 \\
& + m_B^2 (2m_C^4 - 15m_C^2 m_D^2 + 10m_D^4)) + m^6 (m_A^2 - m_B^2)^2 \\
& \times (-11m_C^6 + 102m_C^4 m_D^2 - 60m_C^2 m_D^4 + m_B^2 (35m_C^4 - 56m_C^2 m_D^2 + 32m_D^4))) \\
& + 2(m_A^2 - m_B^2)(2m^2 m_C^2 (m_B^2 + m_C^2)(m_C^2 - 2m_D^2) + (m_A^2 - m_B^2) \\
& \times (m_C^2 - m_D^2)(m_C^4 - 2(m_B^2 + 2m_C^2) m_D^2)) \\
& \times \log \left[\frac{(m^2 - m_A^2 + m_B^2)(-m_C^2 + m_D^2)}{m^2 m_C^2} \right] \Bigg) \Bigg) \\
& / \Big((m_A^2 - m_B^2)^3 (m_B^2 - m_C^2)^2 (2m_B^2 + m_C^2)(m_C^2 - m_D^2)^2 (m_C^2 + 2m_D^2) \Big) , \quad \text{(A.24)}
\end{aligned}
$$

$$
\begin{aligned}
C1_{lA1} = \Bigg(& 3m_B^4 m_C^2 \Bigg(\frac{1}{m_B^2 m_C^2} (2m^{10} m_B^4 (-2m_C^6 + 12m_C^4 m_D^2 - 9m_C^2 m_D^4 + 2m_D^6) \\
& + (m_A^2 - m_B^2)^5 (m_B^2 - m_C^2)(m_C^2 - m_D^2)(4m_C^4 m_D^2 \\
& + m_B^2 (-3m_C^4 + 7m_C^2 m_D^2 + 2m_D^4)) + 2m^8 m_B^2 (m_A^2 - m_B^2) \\
& \times (-2m_C^8 + 14m_C^6 m_D^2 - 11m_C^4 m_D^4 + 2m_C^2 m_D^6 \\
& + m_B^2 (9m_C^6 - 44m_C^4 m_D^2 + 30m_C^2 m_D^4 - 8m_D^6)) + m^2 (m_A^2 - m_B^2)^4 \\
& \times (12m_C^6 m_D^2 (m_C^2 - m_D^2) - m_B^2 m_C^2 (m_C^6 + 16m_C^4 m_D^2 - 19m_C^2 m_D^4 + 10m_D^6) \\
& + m_B^4 (3m_C^6 - 10m_C^4 m_D^2 + 5m_C^2 m_D^4 + 10m_D^6)) - m^6 (m_A^2 - m_B^2)^2 \\
& (-4m_C^8 m_D^2 + 4m_C^6 m_D^4 + m_B^4 (28m_C^6 - 116m_C^4 m_D^2 + 71m_C^2 m_D^4 - 26m_D^6) \\
& + m_B^2 m_C^2 (-10m_C^6 + 76m_C^4 m_D^2 - 61m_C^2 m_D^4 + 14m_D^6)) + m^4 (m_A^2 - m_B^2)^3 \\
& \times (12m_C^6 m_D^2 (-m_C^2 + m_D^2) + m_B^4 (14m_C^6 - 52m_C^4 m_D^2 + 29m_C^2 m_D^4 - 22m_D^6) \\
& + m_B^2 m_C^2 (-10m_C^6 + 74m_C^4 m_D^2 - 59m_C^2 m_D^4 + 18m_D^6))) \\
& + 2(m_A^2 - m_B^2)(m^2 - m_A^2 + m_B^2)^3 (2m^2 m_C^2 (m_B^2 + m_C^2)(m_C^2 - 2m_D^2) \\
& + (m_A^2 - m_B^2)(m_C^2 - m_D^2)(m_C^4 - 2(m_B^2 + 2m_C^2) m_D^2)) \\
& \times \log \left[\frac{(m_B^2 - m_A^2) m_C^2}{m_B^2 (m^2 - m_A^2 + m_B^2)} \right] \Bigg) \Bigg) / \Big((m_A^2 - m_B^2)^3 (m^2 - m_A^2 + m_B^2)^3 \\
& (m_B^2 - m_C^2)^2 (2m_B^2 + m_C^2)(m_C^2 - m_D^2)^2 (m_C^2 + 2m_D^2) \Big) . \quad \text{(A.25)}
\end{aligned}
$$

VFSV:

$$
C1_f = \frac{m_B^2}{\left(-m_A^2 + m_B^2\right)\left(-m_B^2 + m_C^2\right)} , \quad \text{(A.26)}
$$

$$C1_n = \frac{2m_B^2 m_C^2 \left(-\left(m_B^2 - m_C^2\right)\left(m_C^2 - 2m_D^2\right) + 2m_C^2\left(m_B^2 - 2m_D^2\right)\log\left[\frac{m_B}{m_C}\right]\right)}{\left(m_A^2 - m_B^2\right)\left(m_B^2 - m_C^2\right)^2\left(m_C^4 + m_C^2 m_D^2 - 2m_D^4\right)}\,, \quad \text{(A.27)}$$

$$\begin{aligned} C2_n = -\Bigg(& 2m_B^2 m_C^4 \Bigg((m_C^2 - 2m_D^2)(m^2 m_B^2 - (m_A^2 - m_B^2)(m_C^2 - m_D^2)) \\ & + (m_A^2 - m_B^2)(m_B^2 - 2m_D^2)(-m_C^2 + m_D^2) \\ & \times \log\left[\frac{m^2 m_B^2}{(m_A^2 - m_B^2)(m_C^2 - m_D^2)}\right]\Bigg)\Bigg) \\ & / \left(\left(m_A^2 - m_B^2\right)^2\left(m_B^2 - m_C^2\right)^2\left(m_C^2 - m_D^2\right)^2\left(m_C^2 + 2m_D^2\right)\right)\,, \end{aligned} \quad \text{(A.28)}$$

$$\begin{aligned} C1_{hA11} = \Bigg(& m_B^2 m_C^4 \Bigg(m^2(2m^6 m_B^2(m_C^2 - 2m_D^2) - 2(m_A^2 - m_B^2)^3(m_C^2 - m_D^2) \\ & \times (m_B^2 - 2m_C^2 + 2m_D^2) - m^4(m_A^2 - m_B^2)(-3m_C^4 + 4m_C^2 m_D^2 \\ & + m_B^2(7m_C^2 - 12m_D^2)) + m^2(m_A^2 - m_B^2)^2(-9m_C^4 + 16m_C^2 m_D^2 - 4m_D^4 \\ & + m_B^2(7m_C^2 - 10m_D^2))) - 4(m_A^2 - m_B^2)(m^2 - m_A^2 + m_B^2)^3 \\ & \times (m_B^2 - 2m_D^2)(m_C^2 - m_D^2)\mathrm{arccoth}\left[\frac{m^2 - 2m_A^2 + 2m_B^2}{m^2}\right]\Bigg)\Bigg) \\ & / \Big((m_A^2 - m_B^2)^2(m^2 - m_A^2 + m_B^2)^3(m_B^2 - m_C^2)^2 \\ & \times (m_C^2 - m_D^2)^2(m_C^2 + 2m_D^2)\Big)\,, \end{aligned} \quad \text{(A.29)}$$

$$\begin{aligned} C2_{hA12} = \Bigg(& 2m_B^2 m_C^4 \Bigg(\frac{1}{2(m^2 - m_A^2 + m_B^2)^3 m_C^2}(2m_B^2(-m_A^2 + m_B^2)^3 \\ & \times (m_C^4 - 3m_C^2 m_D^2 + 2m_D^4) + m^6(3m_C^6 - 4m_C^4 m_D^2 \\ & + m_B^2(m_C^4 - 6m_C^2 m_D^2 + 4m_D^4)) + 2m^2(m_A^2 - m_B^2)^2(2(m_C^3 - m_C m_D^2)^2 \\ & + m_B^2(3m_C^4 - 10m_C^2 m_D^2 + 6m_D^4)) - m^4(m_A^2 - m_B^2) \\ & \times (9m_C^6 - 16m_C^4 m_D^2 + 4m_C^2 m_D^4 + m_B^2(5m_C^4 - 20m_C^2 m_D^2 + 12m_D^4))) \\ & + (m_B^2 - 2m_D^2)(-m_C^2 + m_D^2)\log\left[-\frac{(m^2 - m_A^2 + m_B^2)(m_C^2 - m_D^2)}{m^2 m_C^2}\right]\Bigg)\Bigg) \\ & / \left(\left(m_A^2 - m_B^2\right)\left(m_B^2 - m_C^2\right)^2\left(m_C^2 - m_D^2\right)^2\left(m_C^2 + 2m_D^2\right)\right)\,, \end{aligned} \quad \text{(A.30)}$$

$$
\begin{aligned}
C1_{lA1} = \Bigg(& m_B^2 \Big(-2m^8 m_B^2 m_C^4 (m_C^2 - 2m_D^2) + (m_A^2 - m_B^2)^4 (m_B^2 - m_C^2) \\
& \times (m_C^6 - 6m_C^4 m_D^2 + 7m_C^2 m_D^4 - 2m_D^6) - m^2 (m_A^2 - m_B^2)^3 (m_C^2 - m_D^2) \\
& \times (m_C^6 + 11 m_C^4 m_D^2 - 6 m_C^2 m_D^4 + m_B^2 (m_C^4 - 15 m_C^2 m_D^2 + 6 m_D^4)) \\
& + m^6 (m_A^2 - m_B^2)(-2m_C^8 - 2m_C^6 m_D^2 + 7 m_C^4 m_D^4 - 2 m_C^2 m_D^6 \\
& + m_B^2 (6 m_C^6 - 6 m_C^4 m_D^2 - 7 m_C^2 m_D^4 + 2 m_D^6)) - m^4 (m_A^2 - m_B^2)^2 \\
& \times (-6 m_C^8 - 2 m_C^6 m_D^2 + 17 m_C^4 m_D^4 - 6 m_C^2 m_D^6 \\
& + m_B^2 (4 m_C^6 + 8 m_C^4 m_D^2 - 21 m_C^2 m_D^4 + 6 m_D^6)) \\
& - 2 (m_A^2 - m_B^2)(m^2 - m_A^2 + m_B^2)^3 m_C^4 (m_B^2 - 2 m_D^2)(m_C^2 - m_D^2) \\
& \times \log \left[\frac{(-m_A^2 + m_B^2) m_C^2}{m_B^2 (m^2 - m_A^2 + m_B^2)} \right] \Big) \Bigg) \Big/ \Big((m_A^2 - m_B^2)^2 (m^2 - m_A^2 + m_B^2)^3 \\
& \times (m_B^2 - m_C^2)^2 (m_C^2 - m_D^2)^2 (m_C^2 + 2 m_D^2) \Big) . \qquad \text{(A.31)}
\end{aligned}
$$

SFVS:

$$
\begin{aligned}
C1_f = & \Big(3 m_B^4 (2 m^4 m_B^2 - 2 m^2 (m_A^2 - m_B^2)(m_B^2 - m_C^2) + (m_A^2 - m_B^2)^2 \\
& \times (m_B^2 - m_C^2)) \Big) \Big/ \Big((m_A^2 - m_B^2)^3 (m_B^2 - m_C^2)^2 (2 m_B^2 + m_C^2) \Big) , \qquad \text{(A.32)}
\end{aligned}
$$

$$
\begin{aligned}
C1_n = & - \Bigg(6 m_B^4 m_C^2 \Big((m_B^2 - m_C^2)(-4 m^2 m_C^2 - (m_A^2 - m_B^2)(m_C^2 - m_D^2)) \\
& + 2 m_C^2 (2 m^2 (m_B^2 + m_C^2) + (m_A^2 - m_B^2)(m_C^2 - m_D^2)) \log \left[\frac{m_B}{m_C} \right] \Big) \Bigg) \\
& \Big/ \Big((m_A^2 - m_B^2)^2 (m_B^2 - m_C^2)^2 (2 m_B^2 + m_C^2)(m_C^2 - m_D^2)^2 \Big) , \qquad \text{(A.33)}
\end{aligned}
$$

$$
\begin{aligned}
C2_n = & \Bigg(6 m_B^4 m_C^4 \Big(2 m^4 m_B^2 m_C^2 + m^2 (m_A^2 - m_B^2)(3 m_B^2 - 2 m_C^2)(m_C^2 - m_D^2) \\
& - 3 (m_A^2 - m_B^2)^2 (m_C^2 - m_D^2)^2 - (m_A^2 - m_B^2)(m_C^2 - m_D^2) \\
& \times (2 m^2 (m_B^2 + m_C^2) + (m_A^2 - m_B^2)(m_C^2 - m_D^2)) \\
& \times \log \left[\frac{m^2 m_B^2}{(m_A^2 - m_B^2)(m_C^2 - m_D^2)} \right] \Big) \Bigg) \\
& \Big/ \Big((m_A^2 - m_B^2)^3 (m_B^2 - m_C^2)^2 (2 m_B^2 + m_C^2)(m_C^2 - m_D^2)^3 \Big) , \qquad \text{(A.34)}
\end{aligned}
$$

$$
\begin{aligned}
C1_{hA11} = \Bigg(& 3m_B^4 m_C^4 \Bigg(m^2(6m^8 m_B^2 - 2m^6(m_A^2 - m_B^2)(9m_B^2 + m_C^2) \\
& + m^4(m_A^2 - m_B^2)^2(19m_B^2 + 5m_C^2) - 2(m_A^2 - m_B^2)^4(m_C^2 - m_D^2) \\
& - m^2(m_A^2 - m_B^2)^3(7m_B^2 - m_C^2 + 2m_D^2)) - 2(m_A^2 - m_B^2) \\
& \times (m^2 - m_A^2 + m_B^2)^3(2m^2(m_B^2 + m_C^2) + (m_A^2 - m_B^2)(m_C^2 - m_D^2)) \\
& \times \log\left[1 - \frac{m^2}{m^2 - m_A^2 + m_B^2}\right]\Bigg)\Bigg) / \Big((m_A^2 - m_B^2)^3(m^2 - m_A^2 + m_B^2)^3 \\
& \times (m_B^2 - m_C^2)^2(2m_B^2 + m_C^2)(m_C^2 - m_D^2)^2\Big), \qquad \text{(A.35)}
\end{aligned}
$$

$$
\begin{aligned}
C2_{hA12} = \Bigg(& 3m_B^4 m_C^4 \Bigg(\frac{1}{(m^2 - m_A^2 + m_B^2)^3 m_C^2 (m_C^2 - m_D^2)} \\
& \times \Big(2m^{10} m_B^2 m_C^2(5m_C^2 - 3m_D^2) + 2(m_A^2 - m_B^2)^5(m_B^2 + 2m_C^2)(m_C^2 - m_D^2)^2 \\
& - 2m^8(m_A^2 - m_B^2)m_C^2(-m_C^4 + m_C^2 m_D^2 + 2m_B^2(8m_C^2 - 5m_D^2)) \\
& - 2m^2(m_A^2 - m_B^2)^4(m_C^2 - m_D^2)(9m_C^4 - 7m_C^2 m_D^2 + m_B^2(2m_C^2 - 3m_D^2)) \\
& - m^4(m_A^2 - m_B^2)^3(-25m_C^6 + 39m_C^4 m_D^2 - 14m_C^2 m_D^4 \\
& + m_B^2(11m_C^4 - m_C^2 m_D^2 - 6m_D^4)) + m^6(m_A^2 - m_B^2)^2 \\
& \times (-11m_C^6 + 15m_C^4 m_D^2 - 4m_C^2 m_D^4 + m_B^2(35m_C^4 - 21m_C^2 m_D^2 - 2m_D^4))\Big) \\
& + 2(m_A^2 - m_B^2)(2m^2(m_B^2 + m_C^2) + (m_A^2 - m_B^2)(m_C^2 - m_D^2)) \\
& \times \log\left[-\frac{(m^2 - m_A^2 + m_B^2)(m_C^2 - m_D^2)}{m^2 m_C^2}\right]\Bigg)\Bigg) \\
& / \Big((m_A^2 - m_B^2)^3(m_B^2 - m_C^2)^2(2m_B^2 + m_C^2)(m_C^2 - m_D^2)^2\Big), \qquad \text{(A.36)}
\end{aligned}
$$

$$
\begin{aligned}
C1_{lA1} = \Bigg(& 3m_B^4 \Bigg(- (m_A^2 - m_B^2)^5 (m_B^2 - m_C^2)(3m_C^4 - 4m_C^2 m_D^2 + m_D^4) \\
& + 2m^{10} m_B^2 (-2m_C^4 - 2m_C^2 m_D^2 + m_D^4) - m^6 (m_A^2 - m_B^2)^2 \\
& \times (-10m_C^6 - 16m_C^4 m_D^2 + 7m_C^2 m_D^4 + m_B^2 (28m_C^4 + 28m_C^2 m_D^2 - 13m_D^4)) \\
& + m^4 (m_A^2 - m_B^2)^3 (-10m_C^6 - 22m_C^4 m_D^2 + 9m_C^2 m_D^4 \\
& + m_B^2 (14m_C^4 + 28m_C^2 m_D^2 - 11m_D^4)) + 2m^8 (m_A^2 - m_B^2) \\
& \times (-2m_C^6 - 2m_C^4 m_D^2 + m_C^2 m_D^4 + m_B^2 (9m_C^4 + 8m_C^2 m_D^2 - 4m_D^4)) \\
& + m^2 (m_A^2 - m_B^2)^4 (m_B^2 (3m_C^4 - 16m_C^2 m_D^2 + 5m_D^4) \\
& - m_C^2 (m_C^4 - 14m_C^2 m_D^2 + 5m_D^4)) + 2(m_A^2 - m_B^2)(m^2 - m_A^2 + m_B^2)^3 \\
& \times m_C^4 (2m^2 (m_B^2 + m_C^2) + (m_A^2 - m_B^2)(m_C^2 - m_D^2)) \\
& \times \log \left[\frac{(1 - \frac{m_A^2}{m_B^2}) m_C^2}{m^2 - m_A^2 + m_B^2} \right] \Bigg) \Bigg) \Big/ \Big((m_A^2 - m_B^2)^3 (m^2 - m_A^2 + m_B^2)^3 \\
& \times (m_B^2 - m_C^2)^2 (2m_B^2 + m_C^2)(m_C^2 - m_D^2)^2 \Big) .
\end{aligned} \tag{A.37}
$$

SFSV:

$$
C1_f = \frac{m_B^2}{\left(-m_A^2 + m_B^2\right)\left(-m_B^2 + m_C^2\right)} , \tag{A.38}
$$

$$
C1_n = \frac{2m_B^2 m_C^2 \left(-m_B^2 + m_C^2 + 2m_B^2 \log\left[\frac{m_B}{m_C}\right]\right)}{\left(m_A^2 - m_B^2\right)\left(m_B^2 - m_C^2\right)^2 \left(m_C^2 - m_D^2\right)} , \tag{A.39}
$$

$$
\begin{aligned}
C2_n = - \Bigg(& 2m_B^2 m_C^2 \Bigg(m_C^2 (m^2 m_B^2 - (m_A^2 - m_B^2)(m_C^2 - m_D^2)) \\
& + m_B^2 (-m_A^2 + m_B^2)(m_C^2 - m_D^2) \log \left[\frac{m^2 m_B^2}{(m_A^2 - m_B^2)(m_C^2 - m_D^2)} \right] \Bigg) \Bigg) \\
& \Big/ \Big((m_A^2 - m_B^2)^2 (m_B^2 - m_C^2)^2 (m_C^2 - m_D^2)^2 \Big) ,
\end{aligned} \tag{A.40}
$$

$$
\begin{aligned}
C1_{hA11} = \Bigg(& m_B^2 m_C^2 \Bigg(m^2 (2m^6 m_B^2 m_C^2 - 2(m_A^2 - m_B^2)^3 (m_B^2 - 2m_C^2)(m_C^2 - m_D^2) \\
& + m^2 (m_A^2 - m_B^2)^2 (-9m_C^4 + 6m_C^2 m_D^2 + m_B^2 (7m_C^2 - 4m_D^2)) \\
& - m^4 (m_A^2 - m_B^2)(-3m_C^4 + 2m_C^2 m_D^2 + m_B^2 (7m_C^2 - 2m_D^2))) \\
& + 2m_B^2 (m_A^2 - m_B^2)(m^2 - m_A^2 + m_B^2)^3 (m_C^2 - m_D^2) \\
& \times \log \left[1 - \frac{m^2}{m^2 - m_A^2 + m_B^2} \right] \Bigg) \Bigg) \Big/ \Big((m_A^2 - m_B^2)^2 (m^2 - m_A^2 + m_B^2)^3 \\
& \times (m_B^2 - m_C^2)^2 (m_C^2 - m_D^2)^2 \Big) ,
\end{aligned} \tag{A.41}
$$

$$
\begin{aligned}
C2_{hA12} = \Bigg(& 2m_B^2 m_C^2 \Bigg((m^6 m_C^2 (m_B^2 + 3m_C^2 - 2m_D^2) \\
& + 2m_B^2 (-m_A^2 + m_B^2)^3 (m_C^2 - m_D^2) + 2m^2 (m_A^2 - m_B^2)^2 \\
& \times (3m_B^2 m_C^2 + 2m_C^4 - 2(m_B^2 + m_C^2) m_D^2) - m^4 (m_A^2 - m_B^2) \\
& \times (9m_C^4 - 6m_C^2 m_D^2 + m_B^2 (5m_C^2 - 2m_D^2))) / (2(m^2 - m_A^2 + m_B^2)^3) \\
& + m_B^2 (m_C^2 - m_D^2) \log \left[\frac{m^2 m_C^2}{(m^2 - m_A^2 + m_B^2)(-m_C^2 + m_D^2)} \right] \Bigg) \Bigg) \\
& / \Big((m_A^2 - m_B^2)(m_B^2 - m_C^2)^2 (m_C^2 - m_D^2)^2 \Big) ,
\end{aligned}
\tag{A.42}
$$

$$
\begin{aligned}
C1_{lA1} = \Bigg(& 2m_B^2 m_C^2 \Bigg(\Big(- 2m^8 m_B^2 m_C^4 + (m_A^2 - m_B^2)^4 (m_B^2 - m_C^2)(m_C^4 - m_D^4) \\
& - m^2 (m_A^2 - m_B^2)^3 (m_C^2 - m_D^2)(m_C^4 - 3m_C^2 m_D^2 + m_B^2 (m_C^2 + 3m_D^2)) \\
& + m^6 (m_A^2 - m_B^2)(-m_C^2 (2m_C^4 - 2m_C^2 m_D^2 + m_D^4) \\
& + m_B^2 (6m_C^4 - 2m_C^2 m_D^2 + m_D^4)) - m^4 (m_A^2 - m_B^2)^2 \\
& \times (-3m_C^2 (2m_C^4 - 2m_C^2 m_D^2 + m_D^4) + m_B^2 (4m_C^4 - 4m_C^2 m_D^2 + 3m_D^4)) \Big) \\
& / \Big(2(m_A^2 - m_B^2)(m^2 - m_A^2 + m_B^2)^3 m_C^2 \Big) + m_B^2 (-m_C^2 + m_D^2) \\
& \log \left[\frac{(m_B^2 - m_A^2) m_C^2}{m_B^2 (m^2 - m_A^2 + m_B^2)} \right] \Bigg) \Bigg) / \Big((m_A^2 - m_B^2)(m_B^2 - m_C^2)^2 (m_C^2 - m_D^2)^2 \Big) .
\end{aligned}
\tag{A.43}
$$

References

[1] T. Appelquist, H. C. Cheng and B. A. Dobrescu, *Phys. Rev.* **D 64** (2001) 035002.

[2] H. C. Cheng, K. T. Matchev and M. Schmaltz, *Phys. Rev.* **D 66** (2002) 056006.

[3] A. Freitas, P. Z. Skands, M. Spira and P. M. Zerwas, *J. High Energy Phys.* **07** (2007) 025.

[4] A. Datta, G. L. Kane and M. Toharia, arXiv:`hep-ph/0510204`.

[5] A. J. Barr, *Phys. Lett.* **B 596** (2004) 205;
J. M. Smillie and B. R. Webber, *J. High Energy Phys.* **10** (2005) 069.

[6] A. Datta, K. Kong and K. T. Matchev, *Phys. Rev.* **D 72** (2005) 096006 [Erratum-ibid. D **72**, 119901 (2005)].

[7] D. J. Miller, P. Osland and A. R. Raklev, *J. High Energy Phys.* **03** (2006) 034.

[8] A. Alves, O. Eboli and T. Plehn, *Phys. Rev.* **D 74** (2006) 095010;
C. Athanasiou, C. G. Lester, J. M. Smillie and B. R. Webber, *J. High Energy Phys.* **08** (2006) 055.

[9] L. T. Wang and I. Yavin, *J. High Energy Phys.* **04** (2007) 032.

[10] C. Kilic, L. T. Wang and I. Yavin, *J. High Energy Phys.* **05** (2007) 052.

[11] C. Csaki, J. Heinonen and M. Perelstein, *J. High Energy Phys.* **10** (2007) 107;
R. Horsky, M. Krämer, A. Muck and P. M. Zerwas, arXiv:0803.2603 [hep-ph].

[12] J. M. Smillie, *Eur. Phys. J.* **C 51** (2007) 933.

[13] M. R. Buckley, H. Murayama, W. Klemm and V. Rentala, arXiv:0711.0364 [hep-ph].

[14] M. R. Buckley, B. Heinemann, W. Klemm and H. Murayama, arXiv:0804.0476 [hep-ph].

[15] A. J. Barr, *J. High Energy Phys.* **02** (2006) 042.

[16] P. Meade and M. Reece, *Phys. Rev.* **D 74** (2006) 015010.

[17] M. Dine, A. E. Nelson and Y. Shirman, *Phys. Rev.* **D 51** (1995) 1362.

[18] G. Burdman, B. A. Dobrescu and E. Ponton, *J. High Energy Phys.* **02** (2006) 033.

[19] G. Burdman, B. A. Dobrescu and E. Ponton, *Phys. Rev.* **D 74** (2006) 075008.

[20] B. A. Dobrescu, K. Kong and R. Mahbubani, *J. High Energy Phys.* **07** (2007) 006.

[21] A. Freitas and K. Kong, *J. High Energy Phys.* **02** (2008) 068.

[22] S. P. Martin, in *Perspectives on supersymmetry*, ed. G. Kane, World Scientific, Singapore (1998) [arXiv:hep-ph/9709356].

[23] E. Ponton and L. Wang, *J. High Energy Phys.* **11** (2006) 018.

[24] I. Hinchliffe and F. E. Paige, *Phys. Rev.* **D 60** (1999) 095002.

[25] Y. Nomura and M. Papucci, *Phys. Lett.* **B 661** (2008) 145;
M. Dine and J. D. Mason, arXiv:0712.1355 [hep-ph];
S. A. Abel, C. Durnford, J. Jaeckel and V. V. Khoze, *J. High Energy Phys.* **02** (2008) 074;
T. Liu and C. E. M. Wagner, arXiv:0803.2895 [hep-ph].

[26] H. C. Cheng, K. T. Matchev and M. Schmaltz, *Phys. Rev.* **D 66** (2002) 036005.

[27] A. Landwehr, Master thesis, University of Zürich (2008).

[28] E. Cremmer, B. Julia, J. Scherk, P. van Nieuwenhuizen, S. Ferrara and L. Girardello, *Phys. Lett.* **B 79** (1978) 231; *Nucl. Phys.* **B 147** (1979) 105;
F. del Águila, A. Culatti, R. Muñoz-Tapia and M. Pérez-Victoria, *Nucl. Phys.* **B 504** (1997) 532.

[29] E. Boos *et al.* [CompHEP Collaboration], *Nucl. Instrum. Meth.* **534** (2004) 250.

[30] D. S. Gorbunov and A. V. Semenov, arXiv:hep-ph/0111291.

[31] T. Sjöstrand, S. Mrenna and P. Skands, *J. High Energy Phys.* **05** (2006) 026.

[32] ATLAS Collaboration, G. Aad *et al.*, *J. Instrum.* **3** (2008) S08003.

[33] E. Richter-Wąs, D. Friodevaux and L. Poggioli, *ATLFAST 2.0 a fast simulation package for ATLAS*, Tech. Rep. ATL-PHYS-98-131, CERN, Geneva, Nov. 1998.

[34] D. Cavalli *et al.*, *Performance of the ATLAS fast simulation ATLFAST*, Tech. Rep. ATL-PHYS-INT-2007-005, ATL-COM-PHYS-2007-012, CERN, Geneva, Jan. 2007.

[35] The ROOT System, http://root.cern.ch;
N. D. Gagunashvili, *Prepared for PHYSTATO5: Statistical Problems in Particle Physics, Astrophysics and Cosmology, Oxford, England, United Kingdom, 12-15 Sep 2005.*